# Anti-biofilm effects and substantively properties of magnetic iron oxide nanoparticles synthesized against clinical isolates for MDR *Acinetobacter baumannii* and related with expression of gene

# Haider Turky Mousa Al-Mousawi\* and Nawar Hadi Al-Janabi

Al – Qasim Green University, College of Biotechnology, Babylon Province, Iraq \*Corresponding author: <a href="mailto:dr.haider.almusawi@biotech.uoqasim.edu.iq">dr.haider.almusawi@biotech.uoqasim.edu.iq</a> Received: October 17<sup>th</sup> 2020; Accepted: November 12<sup>th</sup> 2020

#### **Abstract**

This study aimed to empirical investigation of influence on biofilm formation and determines the gene expression of Bap gene in this bacterial by manufactured of magnetic iron oxide nanoparticles Fe<sub>3</sub>O<sub>4</sub> antibiofilm drug-like. A total of 10 clinical isolates were collected from different sources included (wounds, burns, urine, sputum, blood and throat) that ability to produce strongly biofilm formation. The Fe<sub>3</sub>O<sub>4</sub> NPs was physical-chemical characterized via UV-visible Absorption Spectroscopy, FT-IR, X-RD, AFM and SEM techniques after synthetics by co-precipitation method, the results showed the Fe<sub>3</sub>O<sub>4</sub> NPs have very fine crystalline sizes reach to 11±1 nm by XRD, with mostly spherical in shape and the average size (40- 47) nm nanoparticles by SEM and AFM respectively. The MIC and sub-MIC tests of synthesis Fe<sub>3</sub>O<sub>4</sub> NPs to effect on biofilm formation of A.baumannii isolates at concentrations (15.75 to 2000) µg/ml the results showed that 125µg/ml were MIC and sub-MIC with a significant difference at p>0.05 had been reduced bacterial adhesion inhibitory on polystyrene surface of microtiter plates and consequently caused biofilms. Total RNA were extracted with TRIzol while total RNA was converted to cDNA and the gene expression of biofilm formation Bap normalized gene with housekeeping 16SrRNA gene was conducted by using real-time quantitative PCR assay (RT-qPCR) before and after treated with Fe<sub>3</sub>O<sub>4</sub> NPs. The results showed a significant difference at p>0.05 in Cycle threshold (Ct) values and according to fold regulation equation 2<sup>-(\Delta CT)</sup>) for gene expression for Bap gene of the isolates. Therefore these treatment enhance a significant difference were decreased in gene expression levels of Bap gene and up-regulated at physiological biofilm, without changed with 16SrRNA gene because do not appear any variations of expression before and after treated with Fe<sub>3</sub>O<sub>4</sub> NPs. In this study the synthesized magnetic Fe<sub>3</sub>O<sub>4</sub>NPs with 125μg/ml gave excellent antibiofilm activities and of inhibitory efficiency against A.baumannii isolates; Synthesized magnetic Fe<sub>3</sub>O<sub>4</sub>NPs of the potentiate to down the regulation of gene expression fold for biofilm A.baumannii gene (Bap), leading as a result to have low biofilm production.

Keywords: Acinetobacter baumannii, Biofilm Formation, Fe<sub>3</sub>O<sub>4</sub> NPs, Bap Biofilm gene, Gene expression.

#### Introduction

Acinetobacter spp. is considered as typical opportunistic pathogens with increasing relevance in nosocomial infections worldwide, various risk factors predisposing to severe infection with Acinetobacter genus are believed to have a limited pathogenic potential to otherwise healthy people involved in infections that mainly affect critically ill patients (1;2). On the other hand, in immune compromised patients, several species, in particular Acinetobacter baumannii can cause severe life threatening infections (3;4). A.baumannii infections cause nosocomial infections, and represent the third more frequent species associated with ventilatorassociated pneumonia (VAP), skin and soft-tissue infections, wound infections and catheter-associated urinary tract infections (UTI) and rarely gastrointestinal tract (GIT) infections. A.baumannii and the ninth most frequent species are implicated in the central lineassociated blood stream infections following invasive procedures, and secondary meningitis (1;2).

Emergence of multidrug-resistant bacteria (MDR) A.baumannii in recent years constitutes a significant public health threat. Epidemiological studies and investigation of the prevalence of MDR isolates has also revealed that this problem is growing worldwide (5). Importantly, the increase of MDR isolates of A.baumannii worldwide limite the therapeutic options for treating the infections caused by this MDR pathogen (6). One of the distinctiveness of A.baumanii, which contributes to its extensive survival in the environment is its ability to bioflim formation, or the communities of intercommunicating bacterial cells associated with a surface and encased in an extracellular matrix of carbohydrates, nucleic acids, proteins, and other

macromolecules (7;8). Bacteria have surface structures that are important to initial attachment, which include fimbriae, lipoproteins, lipopolysaccharides, enzymes, and adhesins such Biofilm associated proteins (Bap). Bap aids in the initial attachment and biofilm formation in bacteria on biotic and abiotic surfaces. All Bap bacteria produce strong and adherent biofilms (9). Bap family members are high-molecular weight proteins that are present on the bacterial surface, making it one of the largest bacterial proteins ever described. Bap proteins are generally large (up to 8620 amino acids), and have a signal sequence at their N terminus followed by domains containing a core domain a number of randomly repeated modules A-E. They have a higher proportion of negatively charged amino acids in the tandem repeats compared to non-tandem repeat parts; accordingly they play a critical role in cell-cell interactions and adhesion and biofilm maturation. (10). Over 90% of bacteria are known to live in biofilms, which enable them to reside on surfaces, and build protection mechanisms to prevent eradication by commercial antimicrobials and disinfectants at working concentrations (11). Currently, Magnetic Nanoparticles (MNPs) have many important bioapplications, due to their unique magnetic properties and their ability to function at the molecular and cellular level. They certain MNPs, which are considered an attractive platform for medical applications (12). Iron oxide (y-Fe<sub>2</sub>O<sub>3</sub>) and (Fe<sub>3</sub>O<sub>4</sub>) are the most commonly used MNPs for biomedical applications because biocompatibility and suitable superparamagnetic properties (13). Many researches have observed the effect of iron oxide nanoparticles on bacteria and the inhibition of its activity. For example, iron oxide (Fe<sub>3</sub>O<sub>4</sub>) nanoparticles were shown to reduce viability for types of bacteria by a decrease in the ratio of live to dead cells (14).

Iron oxide nanoparticles may also supply an effective means for a bacterial biofilm treatment on orthopedic implants, or on other medical devices. Penetration of a colloid to any depth in a biofilm is diffusion dependent with an inverse relationship to their size. This is due to the steric and mobility factors while plasma clearance plays a role in decreasing nanoparticle local concentration. Nanoparticles are small enough to penetrate the biofilm. Iron nanoparticles may offer some additional benefits for biofilm treatment (15).

## **Materials and Methods**

**Bacterial Strains:** The Ten of *A.baumannii* clinical strain that strongest biofilm formation was used in this study, were obtained, selected, described and identified previously by (16). These strains were recovered from (Burns, Wounds, Sputum, Urine, Blood and Throat swabs). The strains growth and preservation was carried

out in Luria-Bertani broth (LB) for gene expression experiments.

#### Nanotechnology experiments:

Synthesis of the magnetic iron oxide nanoparticles Fe<sub>3</sub>O<sub>4</sub> NPs: Synthetic of Iron oxide nanoparticles (Fe<sub>3</sub>O<sub>4</sub> NPs) was prepared by the co-precipitation method that described by (17) with modification by (18).

Characterization determination of  $Fe_3O_4$  NPs: The structural and physiochemical properties to measured  $Fe_3O_4$  NPs have been investigated by various tools was carried out of some measurements are the fallowing technique.

- 1-**UV-Visible Absorption Spectroscopy:** The optical Absorbance spectra of the  $Fe_3O_4$  NPs solution were investigated by a double-beam UV-VIS spectrophotometer model (Shimadzu-1). The wavelength range was recorded within the spectral from (295-1100 nm) (19).
- 2- Fourier Transform Infrared (FTIR) Spectroscopy Analysis: The FTIR was a useful to investigate the various functional groups in Fe<sub>3</sub>O<sub>4</sub> NPs was recorded on (FTIR, 8000 Series, Shimadzu) (20). The spectral rang of Fe<sub>3</sub>O<sub>4</sub> NPs was record from wavelength range of numbers (400- 4000) cm<sup>-1</sup>.
- 3-X-Ray Diffraction Spectrum (XRD) Technique: Measured the crystal structure (crystal phases and to determine the crystallite size of phase of Fe<sub>3</sub>O<sub>4</sub> NPs by device type (XRD, 6000- Shimadzu X-ray Diffractmeter) (21).

The grains size was calculated from the width of the XRD peaks, was used to determine the crystallite size using Scherer's equation (22):

 $D = k \lambda / \beta \cos \theta \qquad .....(1)$ 

- **4-Atomic Force Microscopy (AFM):** The characterization of size, surface, roughness, granularity volume distribution and topography of Fe<sub>3</sub>O<sub>4</sub> NPs was measured by (AFM, AA-3000, USA) system model (23).
- 5- Scanning Electron Microscopy (SEM) Analysis: SEM type (Inspect S50. fei company Easy Probe Tescan (Netherlands) is generally used to characterize the morphology properties, microstructure of materials (such as crystal structure, particle shape and size) of Fe<sub>3</sub>O<sub>4</sub> NPs (24).

Determination of minimum inhibitory concentration (MIC) of  $Fe_3O_4$  NPs by Tube Method (TM): The MIC of  $Fe_3O_4$  NPs was determined by a method recommended in (25) with some modifications by (18).

MIC was read as the lowest concentration of iron oxide nanoparticles at which there is tube without visible growth of the bacterial cells (26).

Effects of sub-MIC concentrations of  $Fe_3O_4$  NPs on biofilm formation using Microtiter plate method (27): Overnight *A.baumannii* isolates culture was grown in

brain heart infusion broth. Take 100 µl of bacterial suspension approximate 1.5 ×10<sup>8</sup> cfu/ml was added to the sterile polystyrene microtiter plate with 96 well flatbottom together with 100 µl of different concentration of Fe<sub>3</sub>O<sub>4</sub> NPs, (125) μg/ml in each wells after introduced to the ultrasound bath apparatus to ensure that the nanoparticles did not agglomerate. The control wells contained 180 µl of brain heart infusion broth, and 20 µl of bacterial suspension. Then the culture plates were sealed with para film and were incubated aerobically for 24 h at 37°C. Then non attached bacterial cells were removed and washing the wells and three times with 200 μl of PBS (pH 7.2). After drying at room temperature, 200 µl of crystal violet (0.1%) added to the wells to stain the biofilms which remained adherent to the walls, then incubation for 10 min. The stained attached bacterial cells were rinsed three times with PBS (pH 7.2). Then plates were dried properly at room temperature then adding 200 µl of the distaining solution (95% ethanol) for 10 min. The controls were performed with crystal violet binding to the wells exposed only to the culture medium without bacteria. Then, the microtiter plate were measured the values of OD absorbance at 630 nm. Fe<sub>3</sub>O<sub>4</sub> NPs effects on biofilm by values of optical density (OD) at 630 nm were determined using ELISA Reader (28). The inhibition of biofilm formation percentages of iron oxide nanoparticles for each bacterial isolates was calculated as formal described by (29).

Inhibition efficiency (%) = ((Control OD- test OD)/(Control OD)) ×100% ...... (2)

The microtiter plate antibiofilim assay estimates the percentage of bacterial biofilm reduction, in relative to the control wells, which were set at 100% to indicate the absence of  ${\rm Fe_3O_4}$  NPs. In contrast, negative percentage results indicate no inhibition activity of iron oxide nanoparticles on biofilm organization.

The extraction of RNA and relative quantitative realtime qRT-PCR of Bap gene: Total RNA was extracted from strain colonies for all A.baumannii strain from different sources that giving strongly biofilm formation was done before treatment with the Fe<sub>3</sub>O<sub>4</sub> NPs, extract with an DONGSHENG BIOTECH General RNA Extraction kit (Korea) according the manufacturer's recommendations steps. The RNA concentrations were determined by using NanoDrop Lite Spectrophotometer. Then The RNA was used as a template from which to synthesized cDNA. This standard protocol applies to a single reaction where only template, and water need to be added to the RT FDmix, and the programs used according the manufacturer's recommended. After the PCR program, the synthesis cDNA samples were separated by electrophoresis to shows the band intensity was quantified, Quantification of specific genes listed in Table (1). Thermal Cycler (BioRad Laboratories, Hercules, CA, USA), by using WizOureTM qPCR Master (SYPER) 1-Step RT-qPCR System.

This standard protocol applies to single reaction where only template primers, and water need to be added to the qPCR Master (SYPER) and ROD Dye, with the following cycle profile in Table (2).

Table (1): Oligonucleotides Used to Gene Expression in the Study

Target Gene		Sequence 5′ → 3′	size (bp)	Reference
16SrRNA	F	CAG CTC GTG TCG TGA GAT GT		(30)
	R	CGT AAG GGC CAT GAT GAC TT	150	
	F	TGC TGA CAG TGA CGT AGA ACC		(31)
Вар		ACA	184	
•	R	TGC AAC TAG TGG AAT AGC AGC		
		CCA		

Tabe (2): Thermocycler Program for qRT-qPCR

rabe (2). Thermocycler Program for qivi-qr civ						
Steps	Temperature	Time	Cycles			
Initial Denaturation	95 °C	5 mins	1			
Denaturation	95 °C	15 sec				
Annealing	57 °C	60 sec	40			
Melting curve analysis	95 °C	5 sec / step	1			

The results of data for qRT-PCR calculate as it is a direct comparison of threshold cycles (Ct) values between for target and housekeeping genes were analyzed by the relative quantification gene expression levels (fold change) analysis and one melting curve cycle were analyzed and optimized the  $\Delta\Delta$ Ct method using software that described by (32). The PCR amplification as following equations:

#### ΔCt= Ct target – Ct reference gene.... (3)

 $\Delta\Delta$ Ct = (Ct target – Ct reference) sample – (Ct target – Ct reference) Calibrator ... (4)

Fold change =  $2^{-\Delta\Delta CT}$  ......(5)

So, the relative expression changes in mRNA expression levels were determined using comparative threshold cycle (CT) value method (2<sup>-ΔΔCt</sup>) between the iron oxide nanoparticles treated and untreated for *A. baumannii* isolates.

After adding the Fe<sub>3</sub>O<sub>4</sub> NPs on *Bap* expression: The qRT-PCR was performed to compare the effect of Fe<sub>3</sub>O<sub>4</sub> NPs at appropriate concentration on *Bap* expression gene. Briefly, LB broth tubes  $1\times10^8$ CFU/mL of bacterial cells were inoculated into concentrations of (125) µg/ml of Fe<sub>3</sub>O<sub>4</sub> NPs and incubated for 24 hrs at 37 °C. After that, RNA extraction was done by the same steps by DONGSHENG BIOTECH General RNA Extraction kit. Use same genes, RT master mix and programs that used before add Fe<sub>3</sub>O<sub>4</sub> NPs, and compare the number of isolates that overexpressed *Bap* gene.

**Statistical Analysis**: Statistical analysis system by using computer program (SPSS) was used to analyze the results data, analysis of variance (ANOVA) were used, the level of probability at P values below of  $\leq 0.05$  that used to identify a significant difference (33).

# **Results and Discussion**

**Synthesis of Magnetic Fe<sub>3</sub>O<sub>4</sub> NPs:** The result indicated successfully synthesizing of magnetic iron oxide nanoparticles  $Fe_3O_4$  NPs and show a dark black color with ferromagnetic properties and agreement with (34) them synthesis iron oxide nanoparticles by chemical method.

# Characterization of synthesized Fe<sub>3</sub>O<sub>4</sub> NPs

1- **UV-Vis spectroscopy Assay:** UV-Visible spectroscopy was recorded in the wavelengths rate region between from 290 to 1100 nm) when examined to detect the property of the synthesized Fe3O4 NPs Figure (1). The results of present study shown that a single peak of the Fe3O4 NPs was centered exhibit strong surface plasmon resonance absorption below was recorded at approximately 402 nm, while the absorption edge lies between 312 and 750 nm, indicate the formation and the presence of Fe<sub>3</sub>O<sub>4</sub> NPs. Numerus of reports have established that the resonance peak of Fe<sub>3</sub>O<sub>4</sub> NPs appears around this region, but the correct

position depends on a many factors such particles size and the surface adsorbed species (35).

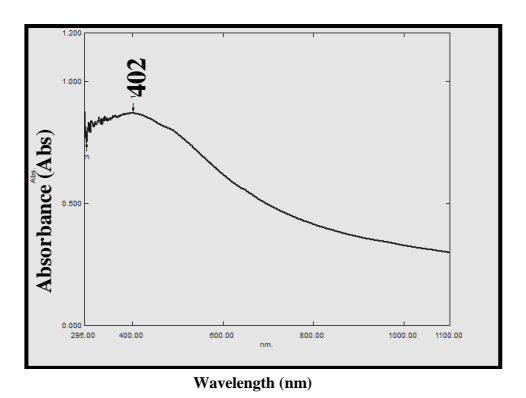


Figure (1): UV-Visible spectral analysis of synthesized (Fe<sub>3</sub>O<sub>4</sub> NPs) recorded maximum absorbance at 402nm

2- Fourier Transform Infrared Spectrum (FTIR) Analysis: The results that obtained by FTIR spectroscopy was shown in Figure (2) that presented the FTIR spectrum of synthesis Fe<sub>3</sub>O<sub>4</sub> NPs with absorption many peaks located in the region between from (4000 cm<sup>-1</sup> to 400 cm<sup>-1</sup>), by strong bands at (3415.70, 2362.64, 1633.59, 1433.01, 1008.70, 630.68, 580.53, 567.03 and 451.31) cm<sup>-1</sup>, corresponds assigned to (hydroxyl group - OH-free, (CH) groups, carbonyl (–C=O) group, phenolic compounds, (COO-) stretching, (C-O) stretch and (C-H) stretching of phenyl ring).

The presence of magnetite  $Fe_3O_4NPs$  can be seen by three strong absorption bands at peaks 580.53, 567.03 and 451.31 cm<sup>-1</sup>, which, corresponding to the Fe-O stretching band of bulk magnetite  $Fe_3O_4$ . The band locations and amounts of absorption peaks are dependent on chemical composition, crystalline structure and also on morphology (36).

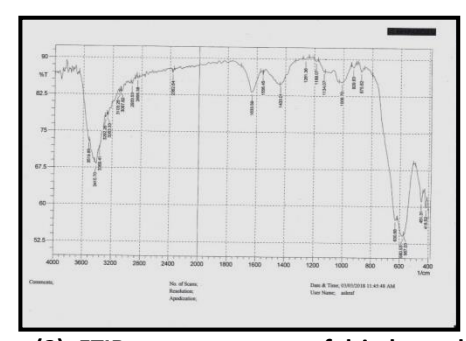


Figure (2): FTIR spectra pattern of dried powder of synthesized Fe<sub>3</sub>O<sub>4</sub> NPs

3- X-Ray diffraction Pattern Measurement (XRD): The result of XRD technique show in Figure (3) there present eight strong with different diffraction peaks corresponding to the crystal planes of crystalline  $Fe_3O_4$  NPs was observed at  $2\theta$  ( $\theta$ =diffraction angle) values of

(30.18°, 35.56°, 43.22°, 53.64°, 57.21°, 62.81°, 70.93° and 74.22°), corresponding to the crystalline distance (d) of (2.95), (2.52), (2.09), (1.70), (1.60), (1.47), (1.32) and (1.27). Bragg reflection, of crystalline  $Fe_3O_4$  NPs respectively. Indicating the black colored magnetic powders are magnetite nanoparticles with spinel phase structure of magnetite. The average crystallite size of the synthesis  $Fe_3O_4$  NPs in current study can be estimated according to the Debye- Scherrer's equation was found to be in the range of (11±1) nm, which gave a correlation between particle size and peak broadening in XRD, that indicated the  $Fe_3O_4$  NPs is very fine. The Sharp peaks also suggest that the  $Fe_3O_4$  NPs have good crystallinity and purity structure. Peak broadening observed is consistent with the small particle size (37).

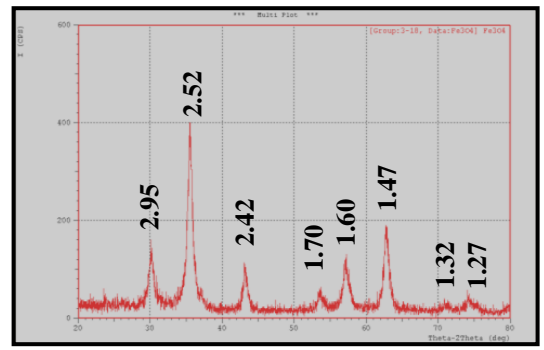


Figure (3): X-ray diffraction pattern of synthesized (Fe<sub>3</sub>O<sub>4</sub> NPs)

**4- Atomic Force Microscope (AFM) Analyses:** The result of AFM Microscopy presented in images shows in Figures (4 A, B) a three-dimensional (3D) and two-dimensional (2D) of a section of the surface of the  $Fe_3O_4$  NPs, demonstrate an smart interaction among  $Fe_3O_4$  NPs leading to the formation of well discrete aggregates, where the high molecular clusters which is up 14.93 nm. The average of diameters and sizes composite of  $Fe_3O_4$  NPs that demonstrate in numerous peaks, the highly peaks is (39) from (8-90) nm. Thus the rate of particles sizes (means of average particle size) of the  $Fe_3O_4$  NPs is 47 nm that shown in Figure (4 C). It is indicating that the  $Fe_3O_4$  NPs synthesis is manufacturing infinitesimal and uniformly arranged.

As the nanoparticles aggregates undergo a Brownian action in suspension, scanning in liquid cannot be used for nanoparticle sizing. Sample preparation is vital in order to get useful AFM images. Samples must be thin enough and must hold fast well to the surface, otherwise the scanning method will producing artifacts (38).

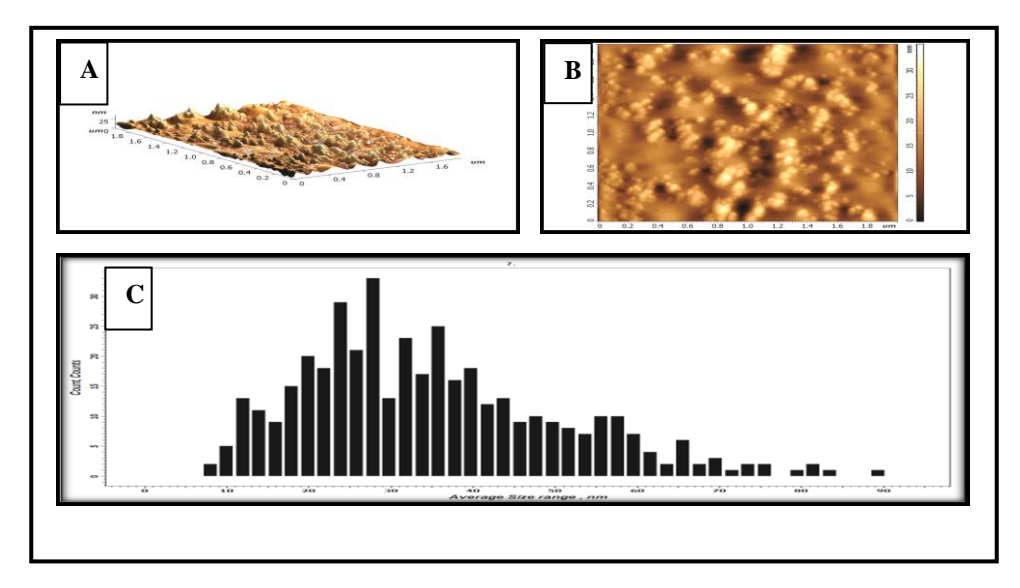


Figure (4): Granularity volume distribution chart Image of the synthesized Fe<sub>3</sub>O<sub>4</sub> NPs by Atomic Force Microscope topographic images (A) Three-Dimensional, (B) Two-Dimensional and (C) Average particle size.

5- Field Emission Scanning Electron Microscope (FE-SEM): SEM images it is evident that the sample consist of by a number quantity of the nanoparticles exhibit spherical shape  $Fe_3O_4$  nanostructures. The average size of the obtained sample approximately 40 nm, indicating

that homogeneous magnetite nanoparticles can be synthesized and rather good size distribution. The crystallites of magnetite particles are less agglomerated shown in Figure (5).

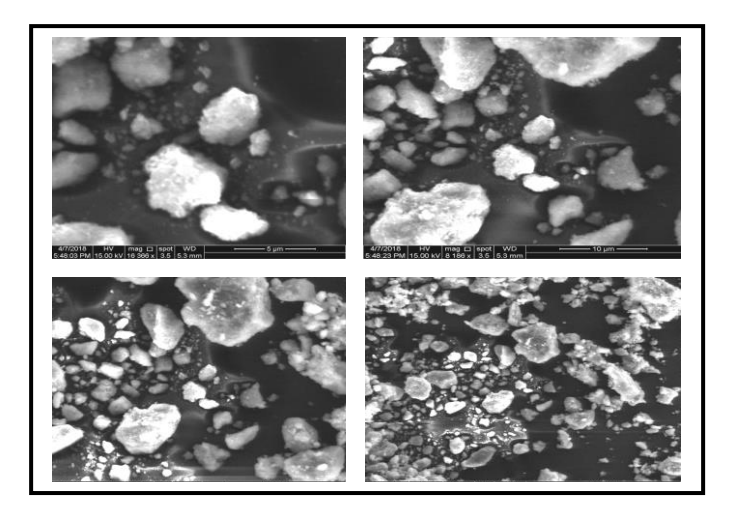


Figure (5): Scanning Electron Microscopy (SEM) images (5, 10, 20 and 50) μm of synthesized Fe<sub>3</sub>O<sub>4</sub> NPs

3. Determination the Minimum Inhibitory Concentration (MIC) Test Results for Fe<sub>3</sub>O<sub>4</sub> Nanoparticles: The result MIC of Fe<sub>3</sub>O<sub>4</sub>NPs for the antibacterial activities in Tube method was presented in Table (3), shown the optical density (O.D) at 630 nm of the means for each concentrations of A.baumannii strain under study, bacterial culture growth in the presence of Fe<sub>3</sub>O<sub>4</sub>NPs compare with (O.D) of the control without NPs. The result showed that the a significant (p<0.05) between concentrations (15.75, 31.25, 62.5, 125, 250, 500, 1000 and 2000) μg /ml of synthesis Fe<sub>3</sub>O<sub>4</sub> NPs that used are demonstrated different result, the lowest concentration give an inhibition the number of cells of 125  $\mu g$  /ml concentration, therefore was the best-used concentration of Fe<sub>3</sub>O<sub>4</sub> NPs for inhibiting growth of *A.baumannii* isolates.

The mode action of the  $Fe_3O_4$  nanoparticles materials were interpreted in terms of the following series process: adsorption onto the bacterial cell surface, diffusion through the cell wall, binding to the cytoplasmic membrane and release of cytoplasmic constituent such as K+ ion, DNA, RNA, and death of the cell (39).

concentration of Fe₃O₄ NPs	Values of O.D at 630 nm			
2000	-			
1000	-			
500	-			
250	-			
125	0.393			
62.5	0.454			
31.25	0.677			
15.75	0.698			
Control	0.722			
LSD value	0.209 *			
(P-value)	(0.0394)			
* (P<0.05).				

Table (3): MIC of Concentration of Fe<sub>3</sub>O<sub>4</sub> NPs

4. The Effect of sub-MIC of iron oxide nanoparticles  $Fe_3O_4$  NPs on antibiofilm by Microtiterplate method: The results showed that the sub-MIC of  $Fe_3O_4$ NPs was 125 µg /ml concentration exhibited a significant reduction in biofilm growth against all *A.baumannii* strain by the absorbance values was decreased for all isolates after a treatment with sub-MIC of these  $Fe_3O_4$  NPs, with different thickness degrees the absorbance values compared with absorbance values of control that untreated with  $Fe_3O_4$  NPs Figure (6). These results indicated that there is a significant difference on biofilm formation after treatment with sub MIC of  $Fe_3O_4$  NPs. The sub-MIC of  $Fe_3O_4$  NPs inhibited bacterial adhesion on polystyrene surface and consequently causes biofilms

detachment and this causes decreased in absorbance values of biofilms (40).

Many studies have shown the size dependent antimicrobial and anti-biofilm effects of these nanoparticles and their physico-chemical properties. The small sizes of nanoparticles enables those to penetrate the biofilm matrix and have a high surface to volume ratio, which promotes effective interactions with bacteria and to make contact with bacterial cells cause inhibition of biofilm Furthermore the Fe<sub>3</sub>O<sub>4</sub>NPs inhibited biofilm production by blocking the formation of exopolysachrides (41).

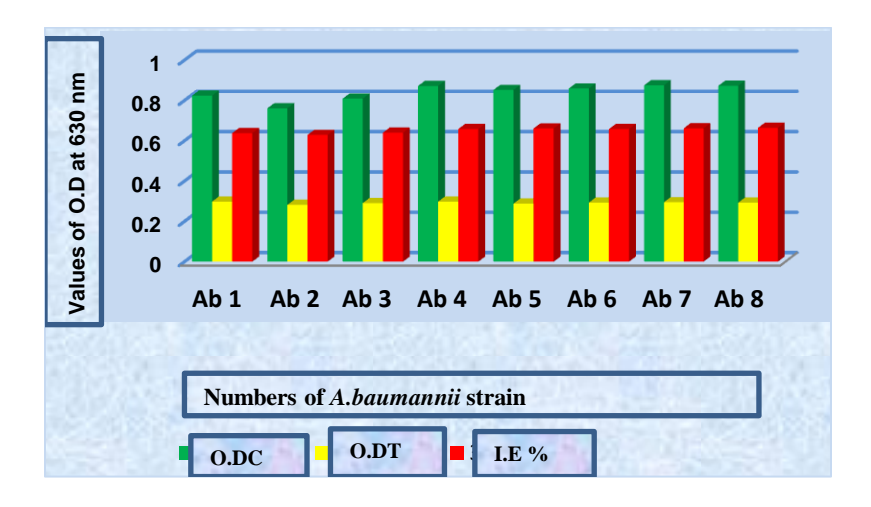


Figure (6): biofilm inhibition activity of Fe<sub>3</sub>O<sub>4</sub> NPs against A.baumannii strain

5. Gene expression analysis by using qRT- PCR technique: Before and after treatment with synthetic  $Fe_3O_4$  NPs, total RNA was carefully extracted by using commercially available RNA extraction for *A.baumannii* isolates. The concentration of total RNA samples 260/280 ratios should be ranged between from (80 to 220) ng/  $\mu$ l. The quality and purity of total RNA samples

ranged between from (1.79 to 2.19)  $ng/\mu l$ , this was measured using Nanodrop ND-2000 spectrophotometer. cDNA reverse transcription was conducted in the same day of RNA extraction, the efficiency of synthesized cDNA concentration was evaluated through gel electrophoresis to identified cDNA band before real time application Figure (7).

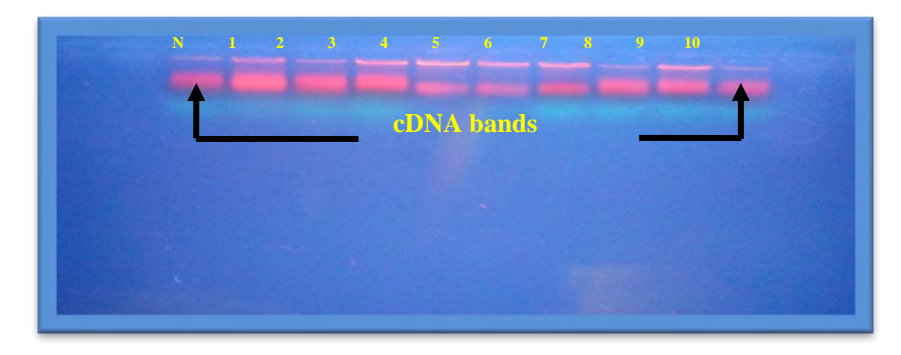


Figure (7): Gel electrophoresis detected cDNA bands from *A.baumannii* isolates (1% agarose,75V, for 30 min stained with ethidium bromide). Lane 1-10: cDNA. Lane N: Negative control (water).

### 6. Real time PCR quantification of Bap gene Expression:

The results of qRT-PCR assay analyzed the mRNA expression of *Bap* gene showed significant variation in gene expression biofilm formation for *A.baumannii* strain. The cycle threshold values (Ct) of *Bap* gene amplification were recorded from the software of qRT-PCR, the statistical analysis shown significant differences according to LSD values at P<0.05 found between the strain, the range from (11.95 to 15.88) before treatment with synthesized Fe<sub>3</sub>O<sub>4</sub> NPs.

The amplification pattern of the gene shown in Figures (8- A and B), these variation submit to differences of the sources of strain.

The results of after treatment with Fe<sub>3</sub>O<sub>4</sub> NPs, the range of Ct value for *Bap* gene from (14.70 to 19.99), there

were significant difference according to LSD values at P<0.05 was found between isolates, the pattern of amplification of this gene showed in Figures (8 - C and D). The melting curve that shown in Figures generated at the end of the PCR reaction show that all amplicon of the *Bap* gene, this result indicates that no primer—dimmers were formed during the reactions.

The statistical analysis also shown significant differences at values P<0.05 in Ct value where comparing between treated and untreated with Fe<sub>3</sub>O<sub>4</sub>NPs for each strain. Expression of the *Bap* gene was decreased in all strain that treated with Fe<sub>3</sub>O<sub>4</sub> NPs, the latter has Ct values were highest than Ct values in untreated, this means decrease gene expression with the increased of Ct values.

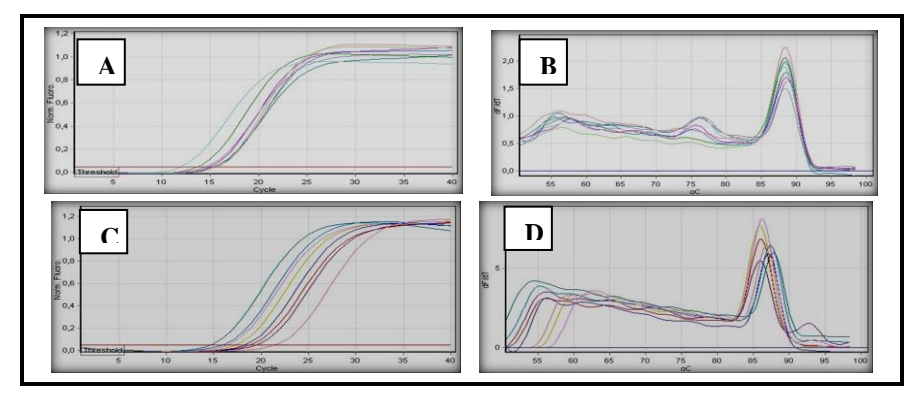


Figure (8): The amplification plots and Melting temperature curve ranged from 85°C to 90°C of *Bap* gene before and after treatment with Fe<sub>3</sub>O<sub>4</sub> NPs

**7. Real time PCR quantification of** *16SrRNA* **gene Expression:** In the current study we used *16SrRNA* is considered the (reference or internal control) gene. The range of Ct value of this gene in case untreated with the  $Fe_3O_4NPs$  from (14.25 to 14.83) in all *A.baumannii* strain, were we then treated with  $Fe_3O_4$  NPs, the Ct value found not changing at high rang from (14.38 to 14.97). The statistical analysis show that non-significant

difference was found between of them strain and between off before and after treatment, the pattern of amplification of the gene shown in Figures (9-A and B) respectively.

The purpose of the reference gene is to normalize the PCRs for the amount of RNA added to the reverse transcription reactions. Standard housekeeping genes usually are sufficient as internal control genes (42).

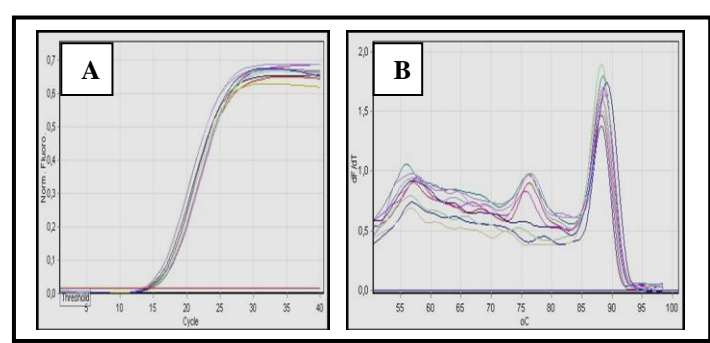


Figure (9): The amplification plots and Melting temperature curve ranged from 85°C to 90°C of 16SrRNA housekeeping gene.

Table (3): Fold of gene expression of Bap gene depending on  $\Delta\Delta$ Ct method.

No.of	Treatment	Ct Bap of	Ct of reference	ΔCt Target	ΔΔCt	2 <sup>-ΔΔCt</sup>
strain		Target gene	16SrRNA	(Ct Bap - Ct		Fold of gene
				internal control		expression
	Untreated	13.70	14.83	- 1.13		
Ab 1	Treated	15.94	14.96	0.98	2.11	0.231
	Untreated	14.97	14.72	0.25		
Ab 2	Treated	17.32	14.88	2.44	2.19	0.219
	Untreated	11.95	14.28	- 2.33		
Ab 3	Treated	14.70	14.58	0.12	2.45	0.183
	Untreated	15.65	14.61	1.04		
Ab 4	Treated	19.57	14.95	4.62	3.58	0.083
	Untreated	13.0	14.25	- 1.16		
Ab 5	Treated	16.50	14.66	1.84	3	0.125
	Untreated	15.35	14.44	0.91		
Ab 5	Treated	18.28	14.65	3.63	2.72	0.151
	Untreated	15.61	14.25	1.36		
Ab 7	Treated	18.83	14.38	4.45	3.09	0.117
	Untreated	15.88	14.62	1.26		
Ab 8	Treated	19.99	14.97	5.02	3.76	0.073
LSD value	(P-value)					0.082* (0.035)
			* (P<0.05).			

Expression of genes associated with biofilm formation ought to be confirmed by genotypic characterization methods. Bap geneswere initially characterized and recognized in A.baumannii. They are characterized by functional qualities and shared structural features involved in these genes that encode the adherence and biofilm formation (43). The main focus in this study on identifying the changes in gene transcription after being treated with  $Fe_3O_4$  NPs. To determine whether Bap expression is actually regulated, qRT-PCR was performed. Indeed, biofilm formation in strain with Bap gene before being treated with synthesized  $Fe_3O_4$  NPs was significantly greater than after being treated with synthesis nanoparticles (p<0.05).

In this study, qRT-PCR determination analyzed the mRNA expression of Bap and 16SrRNA housekeeping gene by compare before and after being treated with  $Fe_3O_4$  NPs for each of the strains. These strains were selective by using a concentration of sub MIC values to  $Fe_3O_4$  NPs to look up at the role of these genes in the biofilm formation of A.baumannii. The calculation of expression fold change was done by using relative quantification from delta delta Ct value ( $\Delta\Delta$ Ct) (42). This depends on normalization of Ct values calculating the  $\Delta$ Ct which is the difference between the mean Ct values of replica of Bap cDNA amplification of each single case and that of the

16SrRNA. The alterations in gene expression levels can be shown in Table (3), which was generated using the data-analysis. This Table show the mean of  $\Delta$ Ct (normalization Ct values) of each strain for Bap gene, depending on evaluate values for Ct of target genes with Ct for internal control. The results of  $\Delta$ CT,  $\Delta\Delta$ CT and  $2^{-\Delta\Delta$ Ct} show that there was a significant difference (P<0.05) in the values between the different studied strains, this difference according to the source of isolated.

To calculate the folds of gene expression of Bap gene in relation to the housekeeping gene, Genes that show significant for the result of 2<sup>-ΔΔCt</sup> values for the strains ranged from (0.073 to 0.231) for Bap gene, these results indicate a significantly decrease expression of biofilm formation after treated with Fe<sub>3</sub>O<sub>4</sub> NPs. These results are consistent given that treated with Fe<sub>3</sub>O<sub>4</sub> NPs causes the growth rate of the bacteria to decrease and decrease genes expressed. The gRT-PCR gene expression study indicated that a number of the genes within the bacterium were upregulated at physiological biofilm. Many previous study about A.baumannii and correlation with adherence and biofilm formation, (44) show Bap expression in A.baumannii population grown in ironlimiting medium, they selected A.baumannii isolates that contained Bap gene and exhibited a strong biofilm formation. They suggested that the low iron Al-Mousawi and Al-Janabi 2021,9(1):122-133.

concentration may play a role in the early biofilm formation.

In a study by (45), they proved the occurrence of *Bap* gene in *A.baumannii* isolates from the whole blood samples. The detection was by a real-time PCR assay. (46) Used polystyrene tube for growing *A.baumannii* showing differences in Biofilm mass, and using specific primers *Bap* and *16SrRNA* genes for the described Gene expression associated with biofilm formation analyzed in both planktonic and sessile conditions. Variation in the expression of factors involved in these pathways may account for the different capacity of bacterial strains to form biofilms and therefore to colonize or infect the host environment (47).

#### Reference

- Shamsizadeh Z.; Mahnaz N.; Bahram N. E. and Hassanzadeh. A. (2017). Detection of antibiotic resistant *Acinetobacter baumannii* in various hospital environments: potential sources for transmission of *Acinetobacter* infections. Environmental Health and Preventive Medicine 22(1).
- Peleg, A. Y.; Seifert, H. and Paterson. D. L. (2008). Acinetobacter baumannii: emergence of a successful pathogen. Clin. Microbiol. Rev., 21:538-582.
- Thomas, J. G.; Slone, W.; Linton, S.; Corum, L. and Percival, S. L. (2012). A comparison of the antimicrobial efficacy of two silver-containing wound dressings on burn wound isolates. Journal of wound care, 20, 580-586.
- Lee, K.; Lee, M. A.; Lee, C. H.; Lee, J.; Roh, K. H.; Kim, S.; Kim, J. J.; Yong, D. and Chong, Y. (2010). Increase of Ceftazidime- and Fluoroquinolone-Resistant *Klebsiella pneumoniae* and Imipenem-Resistant *Acinetobacter spp.* in Korea: Analysis of KONSAR Study Data from 2005 and 2007. Yonsei Med J 51(6):901-911.
- Michalopoulos, A. and Falagas, M. E. (2010). Treatment of *Acinetobacter* infections. Expert Opin. Pharmacother. 11:779–788.
- Shoja, M. M.; Tubbs, R. S.; Shokouhi, G. and Loukas, M. (2017). Wang Qingren and the 19th century Chinese doctrine of the bloodless heart. International Journal of Cardiology, 145(2):305-
- Bardbari, A. M.; Arabestani, M. R.; Karami, M.; Keramat, F.; Aghazadeh, H. and Bagheri, K. P. (2018). Highly synergistic activity of melittin with imipenem and colistin in biofilm inhibition against multidrug-resistant strong biofilm

- producer strains of *Acinetobacter baumannii* Eur. J. Clin. Microbiol. Infect. Dis. pp. 1-12.
- MMcConnell, M. J.; Pérez-Ordóñez, A.; Pérez-Romero, P.; Raquel Valencia. and Jerónimo Pachón. (2018). Quantitative Real-Time PCR for Detection of Acinetobacter baumannii Colonization in the Hospital Environment. Journal of Clinical Microbiology p. 1412–1414.
- Thomas, C. M.; Nielsen, K. M. and Carlier, E. (2016). Mechanisms of and barriers to horizontal gene transfer between bacteria. Nat. Rev. Microbiol. 3, 711–721.
- Loehfelm, T. W.; Luke, N. R. and Campagnari, A. A. (2008). Identification and characterization of *Acinetobacter baumannii* biofilm-associated protein, J Bacteriol.190:1036–1044.
- Giulio, M. D.; Manno, D.; Filippo, E. and Serra, A. (2015). Synthesis and characterization of starch-stabilized Ag nanostructures for sensors applications. Journal of Non-Crystalline Solids, vol. 354, no. 52–54, pp. 5515–5520.
- Tietze, R.; Jurgons, R.; Lyer, S.; Schreiber, E. and Wiekhorst, F. et al. (2014). Quantification of drug-loaded magnetic nanoparticles in rabbit liver and tumour after in vivo administration. J Magn Magn Mater 321: 1465-1468.
- Divine, M. Y.; Ondoh, A. M.; Foba-Tendo, J. and Mbadcam, K. J. (2015). Effect of Decomposition Temperature on the Crystallinity of  $\alpha$ -Fe2O3 (Hematite) Obtained from an Iron (III)-Hexa methylene tetramine Precursor. American Journal of Chemistry, 5(1): 1-9.
- Lee, C.; Kim, J. Y.; Lee, W. I.; Nelson, K. L.; Yoon, J. and Sedlak, D. L. (2008). Bactericidal Effect of Zero-Valent Iron Nanoparticles on *Escherichia coli.*, Environ Sci Technol.42(13): 4927–4933.
- Ansari, M. A.; Khan H. M.; Khan A. A.; Cameotra, S. S.; and Alzohairy, M. A. (2015). Anti-biofilm efficacy of silver nanoparticles against MRSA and MRSE isolated from wounds in a tertiary care hospital. Indian Journal of Medical Microbiology, 33, pp. 101–109.
- Haider, T. AL-Mousawi., Mohammed, I. N. AL-Taee., Qabas, N. AL-Hajjar. (2018). Evaluation of Biofilm Formation Capacity of *Acinetobacter* baumannii Isolated from Clinical Samples in Baghdad Hospitals using Phenotypic Methods, Iraqi Journal of Biotechnology ISSN: 18154794, Volume: 17 Issue: 3 Pages: 47-60.
- Wang, B.; Wei, Q. and Qu, S. (2013). Synthesis and characterization of uniform and crystalline magnetite nanoparticles via oxidation-

- precipitation and modified coprecipitation methods. Int. J. Electrochem. Sci., 8: 3786-3793.
- Haider, T. AL-Mousawi., Mohammed, I. N. AL-Taee., Adil T. Al-Musawi. (2019). Evaluation the Effects of Fe3O4 Nanoparticles on Biofilm Genes Expression Patterns in *Acinetobacter baumannii* using Quantitative Real-Time Polymerase Chain Reaction Assay, Journal of Global Pharma Technology. Vol. 11. Issue 03 (Suppl.) 579-591.
- Meshram, L.; Rakesh, K.P.; Khare, M.; Bagde, S.; Sahare, N.K. and Singh, V. (2012). Comparative analysis between biofilm formation of commensal and pathogenic Escherichia coli isolate. Asiatic Journal of Biotechnology Resources, 3(10): 1441-1446.
- Tsuji, K.; Nakano, K.; Takahashi, Y.; Hayashi, K. and Ro, C.U. (2012). X-ray. The Journal of Infectious Diseases, 215, (supp l-1) 15: S52–S57.
- Cullity B.D and Stock S.R. (2001). Elements of x-ray diffraction, Pearson education, 3rd edition, published by Prentice Hall, 558.
- Hall, J.P.; dobrovolskaia, M.A.; Patri, A.K. and MaNeil, S.E. (2007). Characterization of nanoparticles for therapeutic. Nanomedicine (London).
- Magonov, S.N.; Elings, V. and Whangbo, M.H. (2013). Phase imaging and stiffness in tapping-mode atomic force microscopy. Surf. Sci., 375: 385–391.
- Soares, J. (2014). Optical materials characterization Advanced Materials Spectrometry. Analytical Chemistry. 84: 636–668.
- (CLSI), Clinical and Laboratory Standards Institute. (2013). Performance Standards for Antimicrobial Susceptibility Testing; Twenty-Third Informational Supplement. 33(1): M100-S23.
- Chao, W.; Nan, S.; Zan-Zan, Z.; YangLong, H.; Venkatramana, S.S. and Chuan, X.Z. (2012). Magnetic iron oxide nanoparticles: Synthesis and surface coating techniques for biomedical applications. Chin. Phys. B., 23(3): 037-503.
- Idalina, M.; Graça, J.; Lopes, H.; Lopes, S. and Pereira, M.O. (2013). Antimicrobial Pressure of Ciprofloxacin and Gentamicin on Biofilm Development by an Endoscope-Isolated Pseudomonas aeruginosa. J. Biotechnology, Article ID 178646, 10.
- Gitanjali, K.B. and Dhananjay, K. (2015). Biofilm Producing Multidrug Resistant *Acinetobacter*

- baumannii: An Emerging Challenge. Journal of Clinical and Diagnostic Research, 9(1): DC08-DC10.
- Namasivayam, S.K.R.; Preethi, M.; Bharani, A.R.S.; Robin, G. and Latha, B. (2013). Biofilm Inhibitory Effect of Nanoparticles coated catheter against Staphylococcus aureus and Evaluation of its Synergistic Effects with Antibiotics. Inte. J. Bio. Pharm. Res., 3: 259-265.
- Higgins, P.G.; Wisplinghoff, H.; Stefanik D. and Seifert. H. (2004). Selection of topisomerase mutations and overexpresson of adeB mRNA transcripts during an outbreak of *Acinetobacter baumannii*. J. Antimicrob. Chemother., 54: 821-823.
- Brossard, K. A. and Campagnari, A. A. (2012). The Acinetobacter baumannii biofilm-associated protein plays a role in adherence to human epithelial cells. Infection and immunity. 80 228-
- Schmittgen, T.D.; Lee, E.J.; Jiang, J.; Sarkar, A.; Yang, L.; Elton, T.S., et al. (2008). Real-time PCR quantification of precursor and mature microRNA. Methods, 44: 31-8.
- Urdan, T.C. (2005). Statistics In Plain English, 2nd ed. Lawrence Erlbaum Associates, London: 130-143.
- El-Sigeny, S.M. and Abou Taleb, M.F. (2015). Synthesis, Characterization, and Application of Dendrimer Modified Magnetite Nanoparticles as Antimicrobial Agent. Life Science Journal, 12(6).
- Pal, S.; Tak, Y.K. and Song, J.M. (2007). Does the antibacterial activity of silver nanoparticles depend on the shape of the nanoparticle? A study of the Gramnegative bacterium *Escherichia coli*. Applied and Environmental Microbiology, 73: 1712–1720.
- Zhang, Y.; Dasari, S. T. P.; Deng, H. and Yu, H. (2015). Antimicrobial Activity of Gold Nanoparticles and Ionic Gold. J. Environ Sci. Health C Environ Carcinog Ecotoxicol Rev., 33(3): 286-327.
- Inderam D.C.E.I. and Certu, C.M. (2012). Assesing Fe3O4 nanoparticle size by DLS, XRD and AFM. Journal of optoelectronics and advanced materials, 14(5-6): 460 466.
- Balamurughan, M.G.; Mohanraj, S.; Kodhaiyolii, S. and Pugalenthi, V. (2014). Ocimum sanctum leaf extract mediated green synthesis of iron oxide nanoparticles: spectroscopic and

- microscopic studies. J. of Chemical and Pharmaceutical Sci, 4: 201-204.
- Nayamadi A.M.; Kompany, A. and Mashreghi, M. (2018). Characterization, antibacterial and cytotoxicity studies of graphene-Fe3O4 nanocomposites and Fe3O4 nanoparticles synthesized by a facile solvothermal method. Materials Chemistry and Physics, 213(1): 285-294.
- Parsek, M.R. and Singh, P.K. (2003). Bacterial biofilms: an emerging link to disease pathogenesis. Annu. Rev. Microbiol., 57:677-701.
- Sharmal, P.; Rana, S.; Barick, K.C.; Kumar, C.S.; alunke, H.G. and Hassan, P.A. (2015). Biocompatible phosphate anchored Fe3O4 nanocarriers for drug delivery and hyperthermia. New J. Chem., 5500-5508.
- Schmittgen, T.D.; Lee, E.J.; Jiang, J.; Sarkar, A.; Yang L.; Elton, T.S. *et al.* (2008). Real-time PCR quantification of precursor and mature microRNA. Methods, 44: 31-8.
- Fallah, A.; Rezaee, M. A.; Hasani, A.; Barhaghi, M. H. S. and Kafil, H. S. (2017). Frequency of bap and cpaA virulence genes in drug resistant clinical isolates of *Acinetobacter baumannii* and their role in biofilm formation. Iran J Basic Med Sci, Vol. 20, No. 8.
- Azizi, O.; Fereshteh, S.; Himen, S.; Farzan, M.; Mohammad, R. S. and Vajihe, N. (2016). Molecular Analysis and Expression of bap Gene in Biofilm-Forming Multi-Drug-Resistant Acinetobacter baumannii. Reports of Biochemistry & Molecular Biology Vol.5, No.1.
- De Gregorio E.; Roscetto E.; Iula V. D.; Martinucci, M.; Zarrilli, R. et al. (2015). Development of a real-time PCR assay for the rapid detection of *Acinetobacter baumannii* from whole blood samples. New Microbiol 38: 251–257.
- Selasi, G. N.; Nicholas, A.; Jeon, H.; Na, S.; Oh, M. and Lee, C. (2016). Differences in Biofilm Mass, Expression of Biofilm Associated Genes, and Resistance to Desiccation between Epidemic and Sporadic Clones of Carbapenem Resistant Acinetobacter baumannii Sequence Type 191. PLOSONE | DOI:10.1371/journal.
- Bahador, A.; Farshadzadeh, Z.; Mokhtaran, R. and Hashemi, F.B. (2018). Association of virulence gene expression with colistin-resistance in Acinetobacter baumannii: analysis of genotype, antimicrobial susceptibility, and biofilm

formation. Annals of Clinical Microbiology and Antimicrobials, 17:24.